Biosensors and Bioelectronics 109 (2018) 35–42

Contents lists available at ScienceDirect

Biosensors and Bioelectronics

journal homepage: www.elsevier.com/locate/bios

A universal and label-free impedimetric biosensing platform for discrimination of single nucleotide substitutions in long nucleic acid strands

Dawn M. Mills[a], Christopher P. Martin[a], Stephanie M. Armas[a], Percy Calvo-Marzal[a], Dmitry M. Kolpashchikov[a,b,c,d], Karin Y. Chumbimuni-Torres[a,*]

[a] Department of Chemistry, University of Central Florida, 4000 Central Florida Blvd., Orlando, FL 32816, United States
[b] National Center for Forensic Science, University of Central Florida, Orlando, FL 32816, United States
[c] Burnett School of Biomedical Science, University of Central Florida, Orlando, FL 32816, United States
[d] ITMO University, Laboratory of Solution Chemistry of Advanced Materials and Technologies, Lomonosova St. 9, 191002 St. Petersburg, Russian Federation

ARTICLE INFO

Keywords:
Four-way junction
Electrochemical impedance spectroscopy
Label-free
Universal sensor

ABSTRACT

We report a label-free universal biosensing platform for highly selective detection of long nucleic acid strands. The sensor consists of an electrode-immobilized universal stem-loop (USL) probe and two adaptor strands that form a 4J structure in the presence of a specific DNA/RNA analyte. The sensor was characterized by electrochemical impedance spectroscopy (EIS) using $K_3[Fe(CN)_6]/K_4[Fe(CN)_6]$ redox couple in solution. An increase in charge transfer resistance (R_{CT}) was observed upon 4J structure formation, the value of which depends on the analyte length. Cyclic voltammetry (CV) was used to further characterize the sensor and monitor the electrochemical reaction in conjunction with thickness measurements of the mixed DNA monolayer obtained using spectroscopic ellipsometry. In addition, the electron transfer was calculated at the electrode/electrolyte interface using a rotating disk electrode. Limits of detection in the femtomolar range were achieved for nucleic acid targets of different lengths (22 nt, 60 nt, 200 nt). The sensor produced only a background signal in the presence of single base mismatched analytes, even in hundred times excess in concentration. This label-free and highly selective biosensing platform is versatile and can be used for universal detection of nucleic acids of varied lengths which could revolutionize point of care diagnostics for applications such as bacterial or cancer screening.

1. Introduction

A great number of hybridization-based sensors have been explored for the detection of specific DNA or RNA sequences in clinical molecular diagnostics of human diseases, environmental monitoring and food safety (Gerasimova et al., 2014; Sun et al., 2012; Tosar et al., 2010; Zhao et al., 2015). Among various strategies, electrochemical transduction is routinely adopted for nucleic acid detection because of the simplicity, high sensitivity, low cost and portability (Farjami et al., 2011; Liu et al., 2015; Ricci et al., 2007; Wu et al., 2014). First reported by Fan et al. (2003), a class of electrochemical DNA sensors (E-DNA) which included an immobilized stem-loop (SL) probe with a covalently bound redox marker were developed. This class of E-DNA sensors undergo a conformational change upon target binding and the change in current is measured (Lubin et al., 2006.) Other electrochemical constructs of these sensing platforms such as a double-stem (pseudoknot) DNA probe (Cash et al., 2009; Xiao et al., 2007) and triple-stem DNA probe (Xiao et al., 2009) have been developed to address limitations in differentiating single nucleotide substitutions (SNS). Although E-DNA sensors offer good sensitivity, they still fall short when detecting SNS using folded probes despite the improvements made using the double and triple stem DNA probes.

The selectivity of SL folded probes has been improved by the development of multicomponent probes for optical reporters (Gerasimova et al., 2010; Gerasimova et al., 2013). This approach utilizes adaptor strands along with the conventional molecular beacon (MB) probe, a hairpin-folded DNA strand conjugated with a fluorophore and quencher on opposite ends (Tyagi and Kramer, 1996; Kolpashchikov, 2012). The multicomponent approach exhibits improved selectivity in a broad range of temperatures (5–40 °C) compared to the MB or SL probe due to the design of the short analyte-binding arm of one adaptor strand (Gerasimova et al., 2010; Kolpashchikov, 2006; Stancescu et al., 2016). The short analyte binding arm will not bind at the SNS site and will in turn destabilize the 4J structure, resulting in the SL probe to be thermodynamically favored in its hairpin conformation rather than the 4J structure.

* Corresponding author.
E-mail addresses: dmitry.kolpashchikov@ucf.edu (D.M. Kolpashchikov), karin.chumbimunitorres@ucf.edu (K.Y. Chumbimuni-Torres).

https://doi.org/10.1016/j.bios.2018.02.059
Received 3 December 2017; Received in revised form 7 February 2018; Accepted 26 February 2018
Available online 06 March 2018
0956-5663/

We have used this multicomponent approach to detect DNA and RNA targets (~ 22 bases) with the ability to discriminate SNS and have characterized the sensor using voltammetry techniques (Mills et al., 2017). Other electrochemical 4J sensor designs were explored for the analysis of microRNAs (~ 22 bases), but the previous designs involved the use of multiple covalently bound redox labels or enzyme assisted amplification strategies to reach low limits of detections (Labib et al., 2013, 2015). Although many techniques have been developed to overcome challenges with trace analyte detection, the user-friendly aspect has been eliminated as more steps and costs are incorporated to achieve lower limits of detection (Li et al., 2012; Lin et al., 2014). Therefore, electrochemical impedance spectroscopy (EIS) was also investigated for detection of nucleic acids to achieve low limits of detection (fM-aM) without use of additional amplification steps or expensive bound redox markers (Su et al., 2017). EIS is a powerful technique that monitors interfacial changes upon surface modifications (Lee and Shim, 2001; Li et al., 2002; Zhang et al., 2008). A few studies have explored EIS detection of varied analyte lengths, e.g. 17, 21, and 27 base DNA analytes reported by Wang et al. (2013) or PCR products of 90 bases reported by Minaei et al. (2016), but did not focus on how the length of the analyte affected sensor performance. On the other hand, the size of the analyzed nucleic acid should affect sensitivity of EIS since larger analytes bound to the electrode surface should prevent access of redox couple and thus increase the signal in greater extent than smaller analytes.

In this work, we registered EIS signals produced by analytes of varied lengths (22 bases, 60 bases, 200 bases) sensed by electrochemical 4 J platform to explore the performance and the impact of target length on discrimination of SNS, which has not yet been explored. The sensor includes an immobilized universal stem-loop (USL) probe attached to a gold substrate via a thiol bond and two adaptor strands (m and f) as seen in Scheme 1. The adaptor strands have a SL-binding arm and target-binding arm complementary to the target. In the presence of the target, the USL probe changes its conformation to form a bulky 4J structure that serves as a barrier to the redox couple in solution, resulting in a large charge transfer resistance.

The change in electron transfer resistance was used to monitor the hybridization for nucleic acid targets of varied lengths. An equivalent circuit model was used to analyze the performance of the sensor upon fabrication and hybridization with the nucleic acid analytes. The developed multicomponent sensor could be used for an inexpensive, selective and label-free detection of potentially any RNA or DNA analyte of varied length for point of care clinical diagnostics.

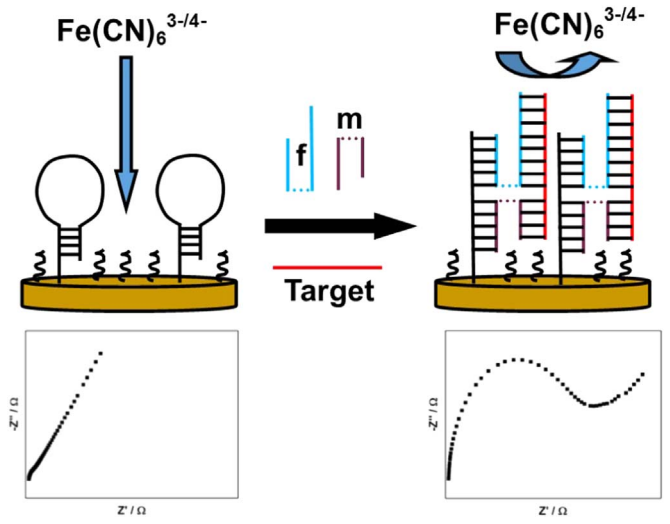

Scheme 1. A schematic of the design of the label-free impedimetric electrochemical 4J sensor.

2. Materials and methods

2.1. Reagents and materials

Tris(2-carboxyethyl phosphine hydrochloride (TCEP), Trizma hydrochloride (Tris-HCl), 6-Mercapto-1-hexanol (MCH) and magnesium chloride ($MgCl_2$) were purchased from Sigma Aldrich (St. Louis, USA). Sodium hydroxide (NaOH), sodium chloride (NaCl), potassium ferrocyanide ($K_4[Fe(CN)_6]$ $3H_2O$), potassium ferricyanide ($K_3[Fe(CN)_6]$), ethanol, hydrogen peroxide (H_2O_2) and sulfuric acid (H_2SO_4) were purchased from Fisher Scientific (Pittsburg, USA). Solutions were prepared with deionized water (18 MΩ cm resistivity) using a Milli-Q Integral Water Purification System from EMD Millipore (Massachusetts, USA). The oligonucleotides used in this study were purchased from Integrated DNA Technologies (Coralville, USA) and used as received (Table 1). An immobilization buffer (IB) was prepared with 50 mM Tris-HCl, 250 mM NaCl. A hybridization buffer (HB) was prepared with 50 mM Tris-HCl, 100 mM NaCl and 50 mM $MgCl_2$. A hybridization buffer (HB) containing bovine serum was prepared with 50 mM Tris-HCl, 100 mM NaCl and 50 mM $MgCl_2$. The buffers were adjusted to a pH of 7.4 using 1 M NaOH.

2.2. Instrumentation

A CHI660D Electrochemical Workstation (CH Instruments, Austin, USA) was used to perform EIS, Cyclic Voltammetry (CV), and Linear Sweep Voltammetry (LSV). Gold screen printed electrodes (DROPSENS, Spain) served as the working electrode (WE) in a three-electrode system which included an external Ag/AgCl (3 M KCl) reference electrode (RE) and platinum counter electrode (CE) (CH Instruments, Austin, USA). EIS, CV, and LSV measurements were recorded in HB containing 5 mM $K_3[Fe(CN)_6]/K_4[Fe(CN)_6]$, this par redox was used since it is very well stablished, characterized and widely used. EIS measurements were taken over a frequency range of 10 kHz to 10 Hz at an AC potential of 0.15 V in a faraday cage to reduce electrical noise. The experimental data is presented as Nyquist plots which were fitted by an equivalent circuit using instrumental software. CV measurements were obtained at a scan rate of 100 mV/s. At least three electrodes were used in each experiment to acquire statistically significant data.

Kinetic studies were performed to calculate the electron transfer rate constant (k_f) at the clean gold electrode, upon USL probe and MCH immobilization, and upon hybridization with the three different target lengths (T-22, T-60 and T-200). Experiments were executed using a gold rotating disk electrode (Au-RDE) of a 5-mm diameter. The electrode was coupled to a modulated speed rotator (MSR) system from PINE Research Instrument, Inc. (Durham, US). Speed rotations were performed from 100 to 3600 rpm.

2.3. Electrode preparation

The WE was activated in 0.5 M H_2SO_4 using CV in the range from 1.6 to − 0.1 V at a scan rate of 100 mV/s. The real surface area of the gold screen printed electrode was calculated from the CVs in sulfuric acid solution by integrating the reduction charge of gold oxide monolayer as described in the literature (Carvalhal et al., 2005; Trasatti et. al, 1991). The WE was then rinsed with DI water and dried with nitrogen prior to use.

2.4. Immobilization and hybridization

The immobilization of the USL probe was achieved using a gold-thiol bond. First, 1 mM TCEP was added to the USL probe and was vortexed for 1 h to reduce the disulfide bonds. This solution was diluted to 0.1 μM in IB and 15 μL of the solution was drop casted and incubated on the electrode for 30 min at room temperature (Mills et al., 2017). Then, the electrodes were rinsed using IB and dried with nitrogen. Next,

Table 1
Nucleic acid sequences.

Strand	Sequence
USL probe	5′-S-S-$(CH_2)_6$-TTTTTTTTTT*CGC**GTTAACATACAATAGATC**GCG* – 3′
f	5′-**GATCTATTGTGTCACACTCCA** – 3′
m	5′-**CAAACACCATTATGTTAAC** – 3′
T-22	5′-**UGGAGUGUGACAAUGGUGUUUG** – 3′
T-60	5′-GTTTCCTTAGCAGAGCTG**TGGAGTGTGACAATGGTGTTTG**TGTCTAAA CTATCAAACGCC – 3′
T-200	5′-CTGACAAGGTTCCCCTATTATCAGTGACAATGGTGGAATGTGGAGGT GAAGTTAACACCTTCGTGGCTACAGAGTTTCCTTAGCAGAGCTG**TGGAGTGTGACAATGGTGTTTG**TGTCTAAACTATCAAACGCCATTATCACACT AAATAGCTACTGCTAGGCAATCCTTCCCTCGATAAATGTCTTGGCATCGTTTGCTT – 3′
SNS-22-a	5′-**UGGAGUGUGACAAUGGUCUUUG** – 3′
SNS-22-b	5′-**UGGAGUGUGACAAUGGUGCUUG** – 3′
SNS-22-c	5′-**UGGAGUGUGACAAUGGAGUUUG** – 3′
SNS-60-a	5′-GTTTCCTTAGCAGAGCTG**TGGAGTGTGACAATGGTCTTTG**TGTC TAAACT ATCAAACGCC – 3′
SNS-60-b	5′-GTTTCCTTAGCAGAGCTG**TGGAGTGTGACAATGGAGTTTG**TGTCTAAA CTATCAAACGCC – 3′
SNS-60-c	5′-GTTTCCTTAGCAGAGCTG**TGGAGTGTGACAATGGTGCTTG**TGTCTAAA CTATCAAACGCC – 3′
SNS-200	5′-CTGACAAGGTTCCCCTATTATCAGTGACAATGGTGGAATGTGGAGGT GAAGTTAACACCTTCGTGGCTACAGAGTTTCCTTAGCAGAGCTG**TGGAGTGTGACAATGGTCTTTG**TGTCTAAACTATCAAACGCCATTATCACACT AAATAGCTACTGCTAGGCAATCCTTCCCTCGATAAATGTCTTGGCATCGTTTGCTT – 3′

[1] The bases that compose the stem of the USL probe are in italics; the SNS site is underlined; the hybridized portion of the targets are in bold.

2 mM MCH (15 μL) was drop casted and incubated on the electrode for 30 min to reduce nonspecific adsorption, then rinsed with IB and dried with nitrogen. The target solutions (T-22, T-60, T-200) were diluted in HB to appropriate concentrations, then mixed with 0.25 μM of the m adaptor strand along with 0.5 μM of the f adaptor strand and 15 μL of the mixture solution was drop casted and incubated on the electrode for 90 min (Mills et al., 2017).

2.5. Spectroscopic ellipsometry

Spectroscopic ellipsometry is a valuable optical technique that provides a thickness value for thin transparent films which has been applied to DNA based biosensors before and after hybridization with a target sequence (Gupta and Atanassov, 2011; Herne and Tarlov, 1997; Mills et al., 2017). Here, a V-VASE ellipsometer (J. A. Woollam Co., Lincoln, USA) was used for ellipsometric measurements (300–800 nm) at incident angles of 65°, 70°, and 75°. The experimental data was modeled using the WVASE software package (J. A. Woollam Co.) and evaluated using a mean square error (MSE) where lower MSE values (< 10) indicate decent agreement with the model. An initial measurement was taken on the bare substrate which consisted of glass slide (1.254 mm) layered with 5 nm titanium oxide (TiO) and 100 nm Au (Infolab Inc., Herndon, USA). Measurements were then taken after DNA SL probe immobilization, backfilling with MCH and hybridization with adaptor strands (m and f) and 1 pM T-60 and T-200.

3. Results and discussion

3.1. Electrochemical behavior of a USL probe-modified electrode

EIS was utilized to investigate the changes at the electrode/electrolyte interface upon modification of the WE. Fig. 1A displays the Nyquist plots for the bare electrode (a) modified with USL probe (b) backfilled with MCH (c) and upon hybridization with the adaptor strands and T-22 (1 pM) (d) in the presence of 5 mM $K_3[Fe(CN)_6]/K_4[Fe(CN)_6]$.

The impedance is shown as the sum of the real Z (Z′) and imaginary Z (Z″) components, which represent the resistance and capacitance of the electrochemical cell. The Nyquist plot generates a semicircle representative of the charge transfer resistance (R_{CT}) due to the electron-transfer kinetics of the redox couple at the electrode's surface. The bare electrode is represented by a straight line in the lower frequency region (Fig. 1A, line a). This demonstrates a diffusion-controlled process at the WE for the redox couple $K_3[Fe(CN)_6]/K_4[Fe(CN)_6]$. A small semicircle was observed in the higher frequency region upon immobilization of the USL probe followed by a straight line in the lower frequency region that represents a mixed electron transfer and diffusion-controlled process at the interface (Fig. 1A, line b). Following immobilization of the USL probe, MCH was used to backfill the electrode to reduce nonspecific adsorption and a larger R_{CT} was generated due to inhibition of the electron transfer of the redox couple $K_3[Fe(CN)_6]/K_4[Fe(CN)_6]$ as the surface of the WE was modified (Fig. 1A, line c). Next, the sensor was hybridized with the adaptor strands (m and f) and 1 pM of T-22 (Fig. 1A, line d). The R_{CT} further increased as the formation of the 4J structure probably decreased the electron transfer efficiency of the redox couple ($K_3[Fe(CN)_6]/K_4[Fe(CN)_6]$). Therefore, the change in R_{CT}, which is strongly dependent on any modification of the electrode's surface, such as target binding, was monitored as a signal for the sensor's response. The equivalent circuit model that represents the electrochemical process at the 4J structure sensor/electrolyte interface was used to interpret the impedimetric spectra (Fig. 1B). In this modified Randles circuit, the R_{CT} (dependent on the electron-transfer kinetics of the redox couple to the electrode's surface) is in parallel with a constant phase element (C), which accounts for the Helmholtz double layer and surface roughness between the self-assembled monolayer and solution, and to the Warburg impedance (Z_w), which represents a diffusion-limited electrochemical process. These circuit elements are in series with the solution resistance (R_s).

3.2. EIS detection of varied target lengths

The conformational change of the USL probe upon target binding affects the charge transfer resistance of the redox couple ($K_3[Fe(CN)_6]/K_4[Fe(CN)_6]$) at the surface of the electrode. The USL probe is in a hairpin conformation in the absence of the target (Scheme 1). In the presence of the target and addition of adaptor strands (m and f), the USL probe opens to form a 4J structure. The target-induced conformational change results in a bulky 4 J structure that blocks the redox couple from accessing the surface of the electrode, resulting in an increased resistance. In addition, the resistance is affected by the repulsion between the negatively charged anions of the redox couple with the negatively charged phosphate backbone of the nucleic acid strands. The conformational switch of the USL probe in the presence of the target and adaptor strands was monitored upon incubation with different concentrations of T-22 (0.5, 1.0, 2.5 and 5.0 pM) as shown in Fig. 2A-B. The ΔR_{CT} increased linearly as the concentration of T-22 increased from 0.5 pM to 5 pM (Fig. 2A). To explore the response of the sensor for targets of varied lengths, the sensor was tested separately with a target containing 60 bases (T-60) and 200 bases (T-200) (Fig. 2C-F). Longer targets resulted in a greater increase of resistance (Fig. 2).

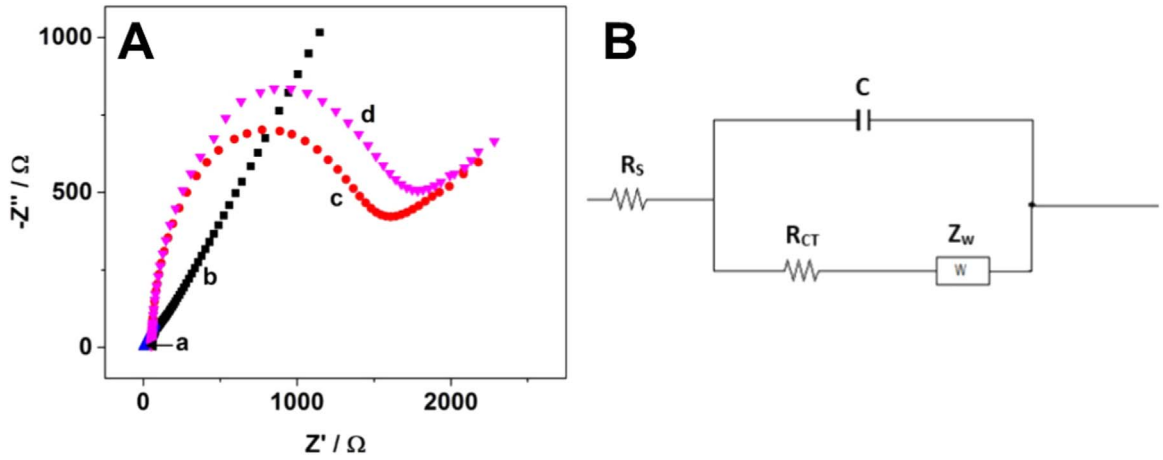

Fig. 1. (A) Nyquist plots of the gold electrode (a) before and (b) after immobilization of the USL probe (c) after backfilling with MCH and (d) upon hybridization with adaptor strands (m and f) and 1 pM target (T-22) in an electrochemical cell containing 5 mM $K_3[Fe(CN)_6]/K_4[Fe(CN)_6]$ and hybridization buffer. The frequency ranged from 10 kHz to 10 Hz at an AC potential of 0.15 V. (B) An equivalent circuit model representing the interface of the electrochemical 4J sensor and electrolyte.

The ΔR_{CT} of the hybridized USL probe increased linearly as the concentration of T-60 increased from 0.1 pM to 5 pM (Fig. 2C) and as the concentration of T-200 increased from 0.01 pM to 5 pM (Fig. 2E).

It is interesting to note that as the length of the target increased from T-22 to T-60, an increase in sensitivity was observed. The slope of the calibration plot for T-22 was 223 Ω/pM and a three-fold increase (650 Ω/pM) was observed for detection of T-60. For T-200 the sensitivity further increased by six-fold (1265 Ω/pM) with respect to T-22. As can be observed, lower limits of detection (LOD) were obtained for longer targets which were calculated as three times the standard deviation of the blank divided by the slope from the calibration curve (S_b/m). The LOD was calculated as 300 fM, 120 fM and 90 fM for T-22, T-60 and T-200, respectively. The difference in the LOD and sensitivities are likely due to increased steric hindrance and surface coverage for longer targets which prohibit the redox couple from achieving an efficient electron transfer.

The corresponding Nyquist plots for the difference in ΔR_{CT} for hybridization of the targets (of different lengths) at a concentration of 1 pM are shown in Fig. 3A. As the length of the target increased, the observed ΔR_{CT} was significantly increased (Fig. 3A). The response for varied target lengths is based on the 4J structure formed, where the longer targets have significantly longer unhybridized portions which act as a barrier to the redox couple in solution, thus increasing the charge transfer resistance. In addition, the longest target (T-200) had a larger linear dynamic range (0.01–5 pM) compared to T-60 (0.1–5 pM) and T-22 (0.5–5.0 pM). This extended linear dynamic range can be attributed to the significantly larger excess portion of the target which reduces charge transfer efficiency of the redox couple in solution, even at low concentrations.

3.3. CV response for varied target lengths

To further investigate the electrochemical processes occurring at the interface, CV was performed from 0.6 to − 0.2 V at a scan rate of 100 mV/s. The cyclic voltammograms are shown in Fig. 3B for 5 mM of $K_3[Fe(CN)_6]/K_4[Fe(CN)_6]$ at the (a) clean electrode (b) upon immobilization of the USL probe and backfilling with MCH and upon hybridization with the adaptor strands and 1 pM of (c) T-22 (d) T-60 or (e) T-200. The peak current decreased and the separation of peak potentials (ΔE_p) increased upon (b) immobilization of the USL probe and backfilling with MCH to 202 ± 8.5 mV as compared to the (a) clean electrode (94 ± 2.2 mV) (Fig. 3B). This is due to the barrier formed by self-assembly bilayer, thus decreasing the access of $K_3[Fe(CN)_6]/K_4[Fe(CN)_6]$ from the bulk solution to the electrode interface. Consequently, the electron transfer efficiency also decreased, as discussed below. The ΔE_p and current are further affected upon hybridization with 1 pM (c) T-22 (267 ± 8.3 mV) (d) T-60 (295 ± 0.82 mV) and (e) T-200 (297 ± 3.3 mV) (Fig. 3B). Once again, these changes are due to the presence of the self-assembled monolayer consisting of the USL probe, the MCH and bulky 4 J structures formed upon hybridization which have a negatively charged phosphate backbone that repel the negatively charged anions of the redox couple while also prohibiting easy access of the redox couple to the surface of the electrode which results in a decrease of electron transfer efficiency. However, the overall change in current and ΔE_p using CV is only slight as the length of the target is increased and is not discernable between T-60 and T-200 indicating that CV is not sensitive enough to discriminate differences in signal with respect to the target length. In contrast, the Nyquist plot (Fig. 3A) shows a clear distinction in signal between the different target lengths (T-22, T-60 and T-200) and demonstrates the benefit of EIS detection when analyzing targets of varied lengths.

3.4. Electron transfer kinetics

The electron transfer rate constant (k_f) was calculated using the Au-RDE clean electrode, upon USL probe and MCH immobilization, and after hybridization with T-22, T-60, and T-200 to form the 4 J bulky structure. The k_f values were determined by LSV, varying the rotation speed of the electrodes before (Figs. S2-S4 in the Supplementary material (SM)) and after immobilization of the USL probe and MCH (Figs. S5-S7 in SM) and then after hybridization with the respective targets (Figs. S8-S10 in SM), for different concentrations of $K_3[Fe(CN)_6]$ (1, 2, 3, 4, 5 mM). The current measured at different rotation speeds was plotted in Koutecky-Levich coordinates (I_L *vesus* $\omega^{-1/2}$) ((Bard et al., 2001) for the electrodes with and without modification. A dependence on diffusion in the reduction process and the involvement of some kinetic step in the electron transfer rate were observed. From the intercept of the Koutecky-Levich graph (Figs. S4, S7 and S10 in SM), the values of I_k for each concentration of $K_3[Fe(CN)_6]$ were obtained and the value of k_f was obtained from the slope in Eq. (1).

$$I_k = nFAk_f C_0^* \quad (1)$$

The value of k_f for the electrode without modification ($k_f = 1.42 \times 10^{-1}$ cm s^{-1}) was larger than those for the electrode upon immobilization of USL probe and MCH ($k_f = 5.01 \times 10^{-3}$ cm s^{-1}) and the electrodes upon hybridization with T-22 ($k_f = 5.18 \times 10^{-3}$ cm s^{-1}), T-60 ($k_f = 6.17 \times 10^{-3}$ cm s^{-1}), and T-200 ($k_f = 5.32 \times 10^{-3}$ cm s^{-1}), which shows that the self-assembled monolayer before and after probe immobilization exerts certain resistance to the electron transfer process. These observations support the EIS results

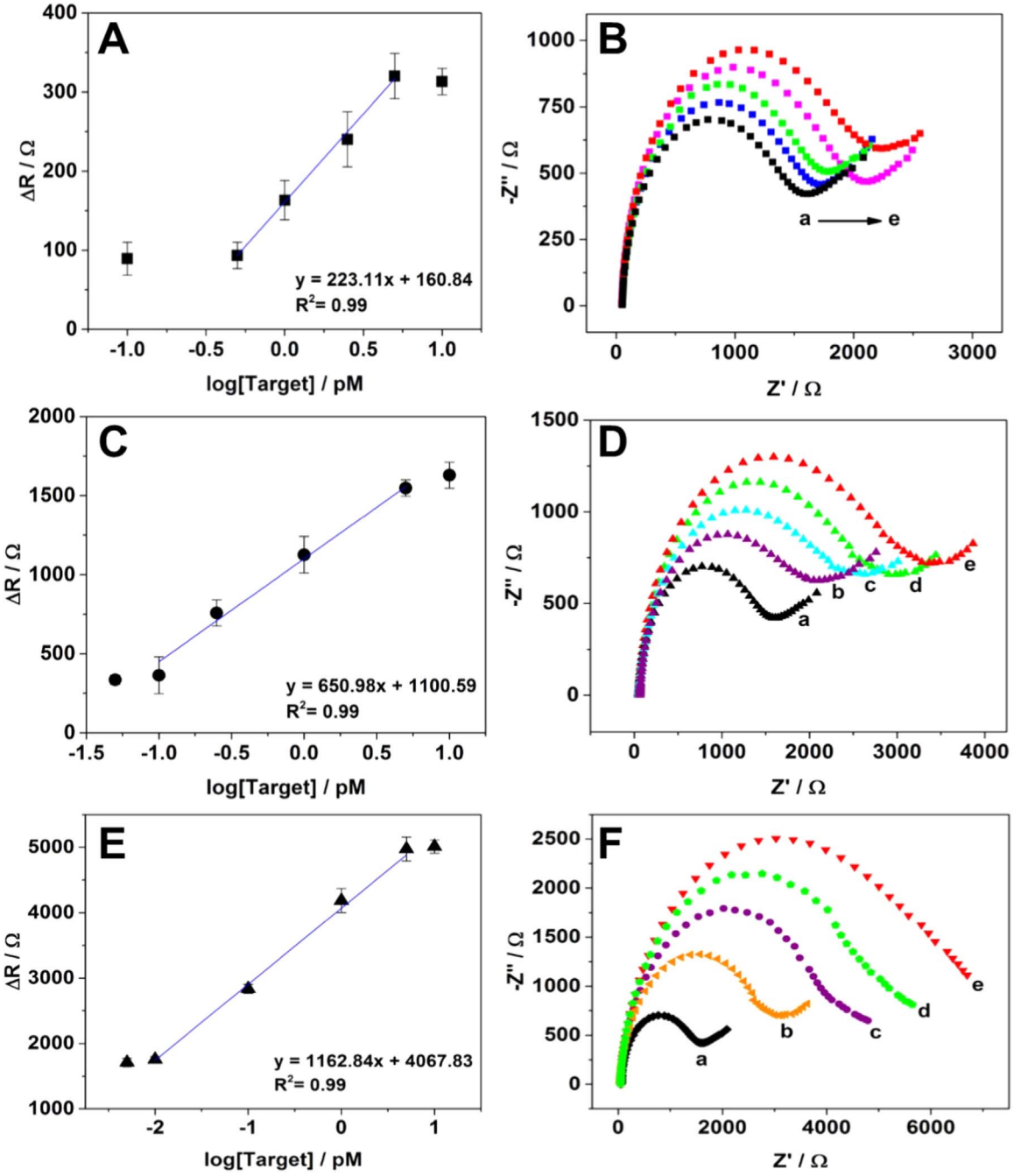

Fig. 2. Analytical performance of the 4J electrochemical sensor. (A) A calibration plot for the ΔR / Ω versus log concentration of T-22. (B) Nyquist plot upon (a) USL immobilization and hybridization of T-22 at concentrations of (b) 0.5 pM (c) 1.0 pM (d) 2.5 pM and (e) 5.0 pM. (C) A calibration plot for the ΔR / Ω versus log concentration of T-60. (D) Nyquist plot upon (a) USL immobilization and hybridization of T-60 at concentrations of (b) 0.1 pM (c) 0.25 pM (d) 1.0 pM and (e) 5.0 pM. (E) A calibration plot for the ΔR / Ω versus log concentration of T-200. (F) Nyquist plot upon (a) USL immobilization and hybridization of T-200 at concentrations of (b) 0.01 pM (c) 0.10 pM (d) 1.0 pM and (e) 5.0 pM.

as the impedance of the electrode without modification shows a linear diffusion process when compared to the electrode modified with USL probe and MCH, which displays a large R_{CT} due to the barrier. Calculated values for k_f at different targets length did not show much difference or correlation, probably due to the small change in the electron transfer process by the different target lengths; similar to the CV response for different targets in Section 3.3. However, the R_{CT} is maximized allowing a clear differentiation between the target lengths.

3.5. DNA layer thickness of varied target lengths

In effort to support the electrochemical experimental data with physical changes (i.e. target-induced conformational change) at the surface of the electrode (SL immobilization, MCH backfilling and hybridization), spectroscopic ellipsometry was utilized to provide thickness of the DNA layer before and after hybridization with targets of different lengths (T-60 and T-200). Upon immobilization of the DNA SL probe and backfilling with MCH, the thickness of the DNA layers were measured as 12.61 ± 0.46 Å and 13.49 ± 0.22 Å respectively, in agreement with our previous study (Mills et al., 2017). Following hybridization with the adaptor strands (m and f) along with T-60 or T-200, the thickness was determined to be 19.12 ± 0.19 Å and 38.60 ± 0.62 Å, respectively. As the target length increased, an increase in thickness was observed. This change in thickness was not as

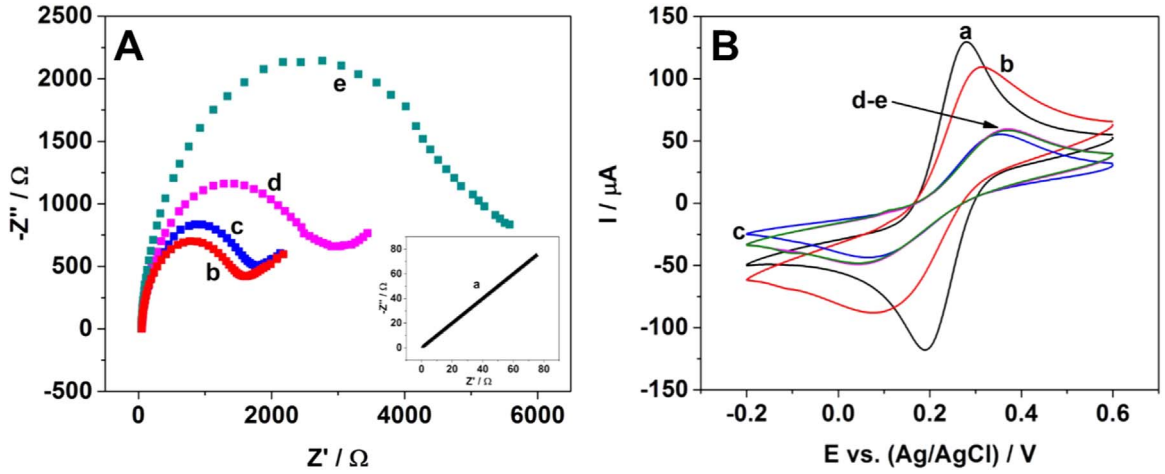

Fig. 3. (A) Nyquist plots and (B) cyclic voltammograms for the (a) clean electrode (b) upon immobilization of 0.1 μM USL probe and backfilling with MCH and hybridization with 0.25 μM m, 0.5 μM f along with 1 pM of (c) T-22 (d) T-60 and (e) T-200.

dramatic as expected, likely due to the low concentration of target used (1 pM). However, at this low concentration, electrochemical behavior is distinct for each target length due to changes at the electrode/electrolyte interface upon target binding. Since there is still a significant change in thickness before and after hybridization with each target, these measurements can provide valuable insight to minute changes of conformation at these low concentration levels in conjunction with electrochemical data.

3.6. Selectivity for varied target lengths

The selectivity of the sensor was studied using EIS upon hybridization of the USL probe with target analytes of varied lengths containing a SNS (SNS-22, SNS-60, SNS-200) along with the adaptor strands (m and f). The R_{CT} for all SNS targets (1 pM) was consistent with that of the DNA SL probe background (Fig. 4, lines a-b). Additionally, even when SNS targets were used in a hundred-fold excess (100 pM), the R_{CT} remained low (Fig. 4, line c) and the signal was similar to the unhybridized sensor. Upon hybridization of the USL probe and adaptor strands with the fully complementary target (T-22, T-60, T-200), a significant change in R_{CT} was observed (Fig. 4d). Furthermore, the selectivity of the sensor was tested for two other locations of the SNS (see Table 1) for two different lengths of target (T-22 and T-60). The R_{CT} for those SNS targets (SNS-22-b, SNS-22-c, SNS-60-b, SNS-60-c) in a hundred-fold excess (100 pM) was consistent with that of the DNA SL probe background (Fig. 4D-E). Upon hybridization of the USL probe and adaptor strands with 1 pM of the fully complementary target (T-22, T-60) a significant change in R_{CT} was observed (Fig. 4D-E, e). These results further support the high selectivity of the sensing platform as the SNS position on the target changes, since the response remains equivalent to the background. Finally, the performance of the sensor was also evaluated towards mixtures containing perfect match and excess of mismatched strands (Fig. 4F). Thus, the sensor was evaluated upon hybridization with variable concentrations of target (T-60): (b) 0.1 pM (c) 5 pM and (d) 15 pM in the presence of 100 pM SNS-60-b (Fig. 4F). As the concentration of the fully complementary target (T-60) was increased, higher R_{CT} were observed, similarly to the behavior observed in the absence of SNS. It is worth emphasizing here that the concentration of SNS is up to 1000 times higher when 0.1 pM fully complementary target was used. Thus, a calibration curve was generated for T-60 in the presence of excess SNS (Fig. S10) which exhibits a slope of 560 Ω/pM and a LOD of 100 fM. When compared to the detection of T-60 in buffer alone, the LODs are both comparable (around 100 pM). However, there is a slight decrease in sensitivity in the detection of T-60 in the presence of excess mismatch versus that in buffer alone 650 Ω/pM (Fig. 2,c) versus 560 Ω/pM, likely due the presence of excess SNS targets in solution. The high degree of selectivity of the electrochemical 4J sensor is due to its unique design. The m adaptor strand possesses a short target-binding arm that prohibits formation of the 4J structure (destabilizes the 4J structure) in the presence of an analyte containing a single nucleotide substitution (Gerasimova et al., 2010; Kolpashchikov, 2006; Stancescu et al., 2016). The results shown here are consistent with our previous studies (Kolpashchikov, 2010; Mills et al., 2017; Nguyen et al., 2011) using the 4J structure (in solution and immobilized) to demonstrate the potential for single base mismatch differentiation. This work shows for the first time the discrimination of SNS for long nucleic acid targets using the electrochemical 4J sensor.

3.7. Specificity of the sensor in BSA

To investigate the specificity of the sensor, the EIS response upon hybridization of T-60 was investigated in a complex matrix containing 40 g/L bovine serum albumin (BSA) in hybridization buffer. The response upon immobilization of the USL probe and MCH (Fig. S11a) was equivalent to the response observed for hybridization with a BSA (containing no target) (Fig. S11b), which indicates the matrix is not adsorbing to the surface of the electrode. The sensor response upon hybridization of T-60 increased, as the concentration of target increased from (c) 0.1 pM (d) 1 pM to (e) 15 pM (Fig. S11) in the BSA matrix. The sensor response is less than observed in buffer alone which could indicate BSA effects, but the signal still increases with respect to the target concentration and the response can be differentiated from the blank BSA matrix. The corresponding calibration curve (slope of 225 Ω/pM) is shown in Fig. S12 and the LOD was calculated to be 400 fM. Although the LOD in the presence of BSA decrease about a 3-fold when compare to no BSA (120 fM), the signal still increases with respect to the target concentration and the response can be differentiated from the blank BSA matrix. These findings suggested BSA effects for the detection of the target but demonstrate the universal sensing platform can potentially be used in complex biological matrices.

4. Conclusions

In this work, we show the development of a novel, label-free electrochemical sensor for the detection of multiple nucleic acid sequences of different lengths with a low limit of detection and capability to be used for SNS differentiation. The principle of this sensing platform relies on the conformational change of a USL probe to form a bulky 4J structure in the presence of the analyte which leads to detectable

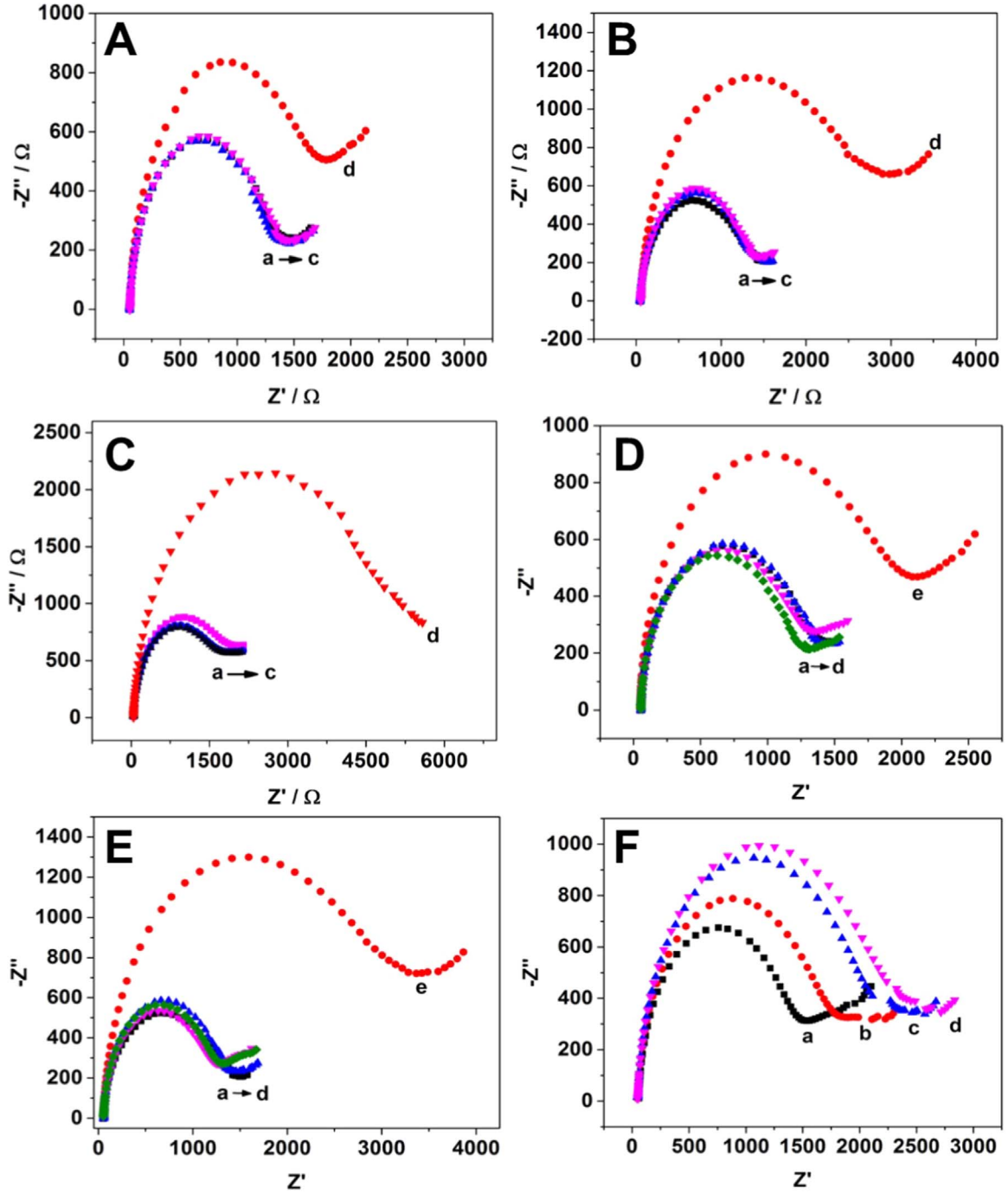

Fig. 4. Sensor response upon (a) immobilization of 0.1 μM USL probe and MCH along with 0.25 μM m and 0.5 μM f for hybridization with (A) SNS-22 at concentrations of (b) 1 pM (c) 100 pM and (d) 1 pM fully complementary target (T-22) (B) SNS-60 at concentrations of (b) 1 pM (c) 100 pM and (d) 1 pM fully complementary target (T-60) (C) SNS-200 at concentrations of (b) 1 pM (c) 100 pM and (d) 1 pM fully complementary target (T-200) (D) 100 pM of (b) SNS-22-a (c) SNS-22-b (d) SNS-22-c and (e) 1 pM fully complementary target (T-22) (E) 100 pM of (b) SNS-60-a (c) SNS-60-b (d) SNS-60-c and (e) 1 pM fully complementary target (T-60) (F) 100 pM of SNS-60-b in HB with T-60 at concentrations of (b) 0.1 pM (c) 5 pM and (d) 15 pM.

changes in charge transfer resistance at the electrode/electrolyte interface. This work demonstrates that the electrochemical 4J sensor can achieve limits of detection at the femtomolar range for three different targets without the use of complex signal amplification techniques as previously reported. In addition, the sensing platform is sensitive to targets of varied length which is an important aspect for a universal sensor to demonstrate applicability to short analytes such as microRNAs (~ 22 bases) as well as longer analytes such as pathogenic bacteria, which will be used in future studies with this sensing platform. This study also demonstrates the high selectivity of the sensor as varying length targets (containing different SNS sites) were discriminated versus that of a fully complementary target. Even in a mixture of excess SNS target the sensor responded to increasing concentrations of the fully matched target only. Preliminary results show the sensor can differentiate increasing concentration of the synthetic target in a matrix containing BSA, but future work with biological samples (e.g. RNA) are needed to address the current limitation of this system for “real world” applications. We are currently investigating the detection of nucleic acid sequence-based amplification (NASBA) products of clinically relevant viruses using this platform to address and explore these

challenges based on the findings presented here. The unique design of the electrochemical 4J sensor allows a highly selective and universal platform not offered by conventional sensors, eliminating the need to optimize a new SL probe for each new target. The novel sensor presented here combines highly sensitive impedimetric transduction, a universal stem-loop probe for the detection of varied length targets, the absence of exogenous labels and high selectivity which could revolutionize point of care testing.

Acknowledgments

The authors acknowledge NSF-nanobiosensing grant number #1706802 and Florida Health Department grant # 7ZK05, the College of Sciences and the Department of Chemistry at the University of Central Florida for financial support of this research. DMK was supported by NSF CCF grants #1117205, 1423219 and NIH R15AI10388001A1, and the ITMO University Fellowship and Professorship Program R15AI10388001A1.

Conflicts of interest

The authors declare no conflict of interest.

Appendix A. Supplementary material

Supplementary data associated with this article can be found in the online version at http://dx.doi.org/10.1016/j.bios.2018.02.059.

References

Bard, J.A., Faukner, L.R., 2001. Electrochemical Methods, Fundamentals and Applications, Second edition. Wiley, New York.
Carvalhal, R.F., Freire, R.S., Kubota, L.T., 2005. Electroanalysis 17, 1251–1258.
Cash, K.J., Heeger, A.J., Plaxco, K.W., Xiao, Y., 2009. Anal. Chem. 81, 656–661.
Fan, C., Plaxco, K.W., Heeger, A.J., 2003. Proc. Natl. Acad. Sci. USA 100, 9134–9137.
Farjami, E., Clima, L., Gothelf, K., Ferapontova, E.E., 2011. Anal. Chem. 83, 1594–1602.
Gerasimova, Y.V., Hayson, A., Ballantyne, J., Kolpashchikov, D.M., 2010. ChemBioChem 11, 1762–1768.
Gerasimova, Y.V., Kolpashchikov, D.M., 2013. Biosens. Bioelectron. 41, 386–390.
Gerasimova, Y.V., Kolpashchikov, D.M., 2014. Chem. Soc. Rev. 43, 6405–6438.
Gupta, G., Atanassov, P., 2011. Electroanalysis 23, 1615–1622.
Herne, T.M., Tarlov, M.J., 1997. J. Am. Chem. Soc. 119, 8916–8920.
Kolpashchikov, D.M., 2006. J. Am. Chem. Soc. 128, 10625–10628.
Kolpashchikov, D.M., 2010. Chem. Rev. 110, 4709–4723.
Kolpashchikov, D.M., 2012. Scientifica (Cairo). 2012, 928783.
Labib, M., Ghobadloo, S.M., Khan, N., Kolpashchikov, D.M., Berezovski, M.V., 2013. Anal. Chem. 85 (20), 9422–9427.
Labib, M., Khan, N., Berezovski, M.V., 2015. Anal. Chem. 87, 1395–1403.
Lee, T.Y., Shim, Y.B., 2001. Anal. Chem. 73, 5629–5632.
Li, C.M., Song, S., Maracas, G., Choong, V.N., 2002. US Patent, 20020051975.
Li, W., Wu, P., Zhang, H., Cai, C., 2012. Chem. Commun. 48, 7877–7879.
Lin, M., Wen, Y., Li, L., Pei, H., Liu, G., Song, H., Zuo, X., Fan, C., Huang, Q., 2014. Anal. Chem. 86, 2285–2288.
Liu, S., Su, W., Li, Z., Ding, X., 2015. Biosens. Bioelectron. 71, 57–61.
Lubin, A.A., Lai, R.Y., Baker, B.R., Heeger, A.J., Plaxco, K.W., 2006. Anal. Chem. 78, 5671–5677.
Mills, D.M., Calvo-Marzal, P., Pinzon, J.P., Armas, S., Kolpashchikov, D.M., Chumbimuni-Torres, K.Y., 2017. Electroanalysis 29, 873–879.
Minaei, M.E., Saadati, M., Najafi, M., Honari, H., 2016. Electroanalysis 28, 2582–2589.
Nguyen, C., Grimes, J., Gerasimova, Y.V., Kolpashchikov, D.M., 2011. Chemistry 17, 13052–13058.
Ricci, F., Lai, R.Y., Plaxco, K.W., 2007. Chem. Commun. 3768–3770.
Stancescu, M., Fedotova, T.A., Hooyberghs, J., Balaeff, A., Kolpashchikov, D.M., 2016. J. Am. Chem. Soc. 138, 13465–13468.
Su, S., Cao, W., Liu, W., Lu, Z., Zhu, D., Chao, J., Weng, L., Wang, L., Fan, C., Wang, L., 2017. Biosens. Bioelectron. 94, 552–559.
Sun, X., Guan, L., Shan, X., Zhang, Y., Li, Z.J., 2012. Agric. Food Chem. 60, 10979–10984.
Tosar, J.P., Branas, G., Laiz, J., 2010. Biosens. Bioelectron. 26, 1205–1217.
Trasatti, S., Petree, O.A., 1991. Pure Appl. Chem. 63, 711–734.
Tyagi, S., Kramer, F.R., 1996. Nat. Biotechnol. 14, 303–308.
Wang, C., Yuan, X., Liu, X., Gao, Q., 2013. Anal. Chim. Acta 799, 36–43.
Wu, Y., Lai, R.Y., 2014. Anal. Chem. 86, 8888–8895.
Xiao, Y., Lou, X., Uzawa, T., Plakos, K.J.I., Plaxco, K.W., Soh, H.T., 2009. J. Am. Chem. Soc. 131, 15311–15316.
Xiao, Y., Qu, X.G., Plaxco, K.W., Heeger, A.J., 2007. J. Am. Chem. Soc. 129, 11896–11897.
Zhang, K., Ma, H., Zhang, L., Zhang, Y., 2008. Electroanalysis 20, 2127–2133.
Zhao, Y., Wang, H., Tang, W., Hu, S., Li, N., Liu, F., 2015. Chem. Commun. 51, 10660–10663.